Received: 28 February 2019 | Revised: 28 February 2019 | Accepted: 23 April 2019

DOI: 10.1111/ijac.13259

International Journal of Applied Ceramic Technology

ORIGINAL ARTICLE

Facile synthesis of α-Si_3N_4 nanoneedles and their photoluminescence properties

Xiulin Shen | Haitao Liu | Xianmei Zhang | Zhaohui Huang | Yangai Liu | Minghao Fang | Xiaowen Wu | Xin Min

Beijing Key Laboratory of Materials Utilization of Nonmetallic Minerals and Solid Wastes, School of Materials Science and Technology, National Laboratory of Mineral Materials, China University of Geosciences, Beijing, PR China

Correspondence
Xianmei Zhang and Zhaohui Huang, Beijing Key Laboratory of Materials Utilization of Nonmetallic Minerals and Solid Wastes, School of Materials Science and Technology, National Laboratory of Mineral Materials, China University of Geosciences, Beijing 100083, PR China.
Emails: zhangxianmei@chinapowder.com (X. Z.) and huang118@cugb.edu.cn (Z. H.)

Funding information
National Natural Science Foundation of China, Grant/Award Number: No.51472222 51372232; National Key R&D Program of China, Grant/Award Number: 2018YFC1901503

Abstract

Needle-like α-Si_3N_4 with unique structures has potential application in both field emission devices and tips for atomic force microscopes. Single-crystalline, α-Si_3N_4 nanoneedles have been prepared by using an improved chemical vapor deposition (CVD) method at 1200°C for 3 hours. The phases, chemical composition, and microstructure of the as-prepared products were determined by X-ray diffraction (XRD), field emission scanning electron microscopy (FESEM), and transmission electron microscopy (TEM) equipped with EDS. The as-synthesized products show a needle-like morphology with hundreds of micrometers in length and nanometer-featured tips. The nanoneedles show a α-Si_3N_4@SiO_x core-shell heterostructure as characterized by TEM, with single-crystalline α-Si_3N_4 core and an insulating amorphous silicon oxide shell. The growth of α-Si_3N_4 nanoneedles corresponds to vapor-liquid-solid cap-growth and base-growth mechanism. Photoluminescence (PL) properties of the products were also characterized. An obvious emission peak at 400 nm under 254 nm UV excitation was observed. The nanoneedle morphology and photoluminescence properties of the products have potentials to be used in future optoelectronic nanodevices.

KEYWORDS

CVD, growth mechanism, nanoneedles, photoluminescence, α-Si_3N_4

1 | INTRODUCTION

One-dimensional (1D) nanomaterials (nanotubes,[1,2] nanowires,[3,4] nanobelts,[5–7] nanoneedles[8,9]) have drawn great attention in recent decades. Given their high surface-to-volume ratio, 1D nanomaterials have extensive potential to be applied in optical materials,[10–12] ceramics,[13–15] electronics,[16] and biomaterials[17] *etc*.[18–24] Silicon nitride possesses low thermal expansion coefficient.[25,26] high strength and stiffness, high thermal conductivity, outstanding thermal shock resistance,[27] and excellent resistance to wear.[28–30] Besides, α-Si_3N_4 is an important wide band gap semiconductor (5.3 eV), resulting in good optical and electrical properties. α-Si_3N_4 nanomaterials exhibit excellent photoluminescence and thermo-mechanical properties, which make them good candidates for optoelectronic nanodevices, such as UVC photodetectors. By controlling the defects and the SiO_x shell, one can tailor the emission peak of the 1D α-Si_3N_4 nanomaterials. It is worth noting that the photoluminescence peaks and fluorescence intensity can be adjusted by controlling defects in the microstructure of α-Si_3N_4.[5,31]

Traditionally, 1D Si_3N_4 nanomaterials can be prepared by chemical vapor deposition (CVD),[32] plasma-enhanced CVD (PECVD),[33] microwave plasma heating,[9,34] catalytic pyrolysis of a polymer precursor,[35] sol–gel,[4] and combustion synthesis,[36] *etc*. The CVD method is considered to be a potential

method for the synthesis of α-Si_3N_4 nanostructures due to its low cost and simplicity. Currently, a lot of pioneer works presented the synthesis of 1D α-Si_3N_4 nanostructures with various morphologies. Researchers studied on the formation mechanism of α-Si_3N_4 morphology. Liu[28] et al. synthesized α-Si_3N_4 with different micromorphologies using a molten salt nitriding method. It was found that α-Si_3N_4 products include nanowires, blocks, and slender nanobelts. Sodium chloride, β-Si_3N_4, and Si powder were used as raw materials in this method. They believed that different morphologies of products were caused by different concentrations of the raw materials and different heating temperature. Takafumi Kusunose et al. [37] prepared α-Si_3N_4 nanowires by the carbothermal reduction and nitridation of a homogeneous mixture of silica (SiO_2), carbon, and a small amount of cobalt via the vapor-liquid-solid (VLS) mechanism. The epoxy composite containing α-Si_3N_4 nanowires of 60 vol% showed a high thermal conductivity of 9.2 W m^{-1} K^{-1} along the preferred orientation of the nanowires. In traditional VLS-based methods, nanowires with uniformed diameters were grown along the catalyst tip by controlling the concentration of gas precursors. Limited by this process, in the family of 1D α-Si_3N_4 nanostructures, nanoneedles with sharp tip and gradually enlarged diameter were rarely reported.

In this article, we report an improved VLS method to synthesize α-Si_3N_4 nanoneedles without using flowing gases. The phase composition, morphology, and microstructure of the products were characterized. The growth mechanism of the nanoneedles was proposed according to the experimental observations and previous studies. The resulting α-Si_3N_4 nanoneedles were found to show an obvious emission peak at 400 nm under the excitation of 254 nm UV light.

2 | MATERIALS AND METHODS

The experimental equipment consists of a horizontal high-temperature tube furnace and two corundum crucibles (as shown in Figure 1). First of all, an *n*-type Si (100) wafer (1 cm × 1 cm) was ultrasonically cleaned in acetone and ethanol for 20 minutes, respectively, and then air-dried at room temperature. The Si wafer was coated by a layer of Au with 0.5-1 nm thickness. After that, the Au-coated Si substrate was placed in a larger alumina crucible, covered with another smaller corundum crucible as shown in Figure 1. Finally, the bigger crucible was completely filled with silicon powder and sealed with a corundum lid. It was worth noting that the silicon powder we used to fill the space between crucibles is recyclable and reusable. In this way, the Si (100) wafer with Au catalyst is completely separated from another Si source (silicon powder) in case unnecessary distractions occur. The closed system was then placed in a tube furnace and heated in the air atmosphere. The temperature increase mechanism in the furnace is to increase from room temperature to 1000°C at 10°C/min, then from 1000°C to 1200°C at 3°C/min, and to hold at 1200°C for 3 hours. After cooling to room temperature, a white layer of products can be seen on the substrate. It was characterized with an X-ray diffractometer (XRD, D8 Advance, Germany), a field emission scanning electron microscope (FESEM, Quanta FEG 650, America) equipped with an energy dispersive spectroscopy (EDS, INCA), and a transmission electron microscope (TEM, TECNAI G2, America). The room temperature photoluminescence spectra of the products were recorded with a fluorescence spectrophotometer (PL, Hitachi F-4600, Japan) equipped with a 450 W xenon discharge lamp as the excitation source.

3 | RESULTS AND DISCUSSION

In this research, an improved and simplified CVD method without using flowing gases (N_2, CH_4, Ar, NH_3, etc.) was employed to synthesize α-Si_3N_4 nanomaterials. A white layer of thin film can be seen on the Si substrate. Figure 2 shows the X-ray diffraction (XRD) pattern of the products. The peaks with strong intensities and narrow width indicated the products were crystalline. Searching and matching the peaks in the PDF database, the peaks can be

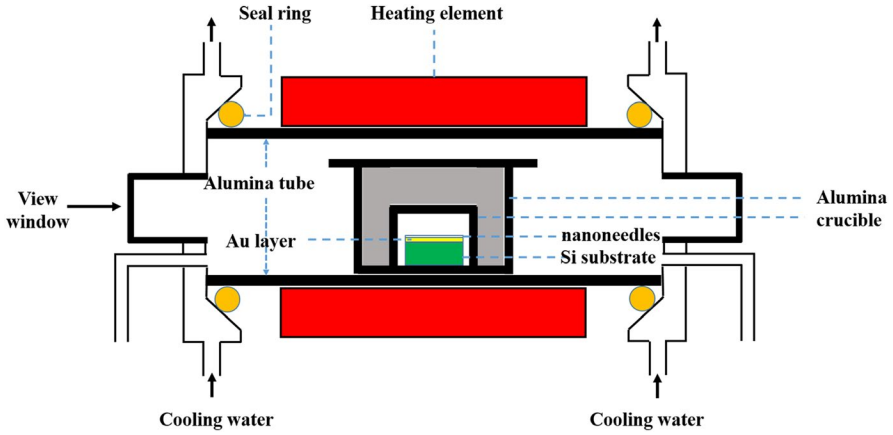

FIGURE 1 Schematic diagram of the experimental equipment for α-Si_3N_4 nanowires preparation [Color figure can be viewed at wileyonlinelibrary.com]

indexed to those of the standard PDF cards (JCPDS Card No: 5-659) of α-Si_3N_4. What's more, there are some peaks corresponding to SiO_2.

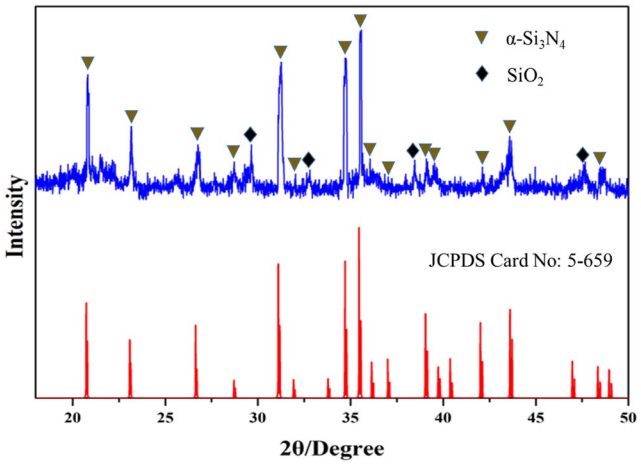

FIGURE 2 XRD pattern of α-Si_3N_4 nanoneedles [Color figure can be viewed at wileyonlinelibrary.com]

Figure 3A-E shows the typical FESEM images of the as-synthesized products. As can be seen, the α-Si_3N_4 products exhibit a tree crown-like divergence, multiple nanoneedles sharing one single root. Their length is in the range of 100-200 μm with excellent uniformity. Figure 3F-G shows high-resolution FESEM images, and the sharp needles with dozens of nanometers to several micrometers through the thin-to-thick shape can be observed. Detailed TEM characterization of the sharp tips is presented in Figure 4. Figure 3H shows a typical image of the needle cap. There are spherical clusters at the needle cap. An EDS spectrum recorded from the needle cap is presented in Figure 3I, which shows that there are only Si and Au elements in the spherical clusters of nanoneedles (N element cannot be seen because it is a light element.). It indicates that Au, as the catalyst, accelerates the growth of the top. Together with the XRD and EDS results, we confirmed that the as-formed nanoneedles were α-Si_3N_4.

The as-prepared α-Si_3N_4 nanoneedles were further characterized by transmission electron microscopy (TEM). After sonicated and suspended in pure ethanol, the solution was

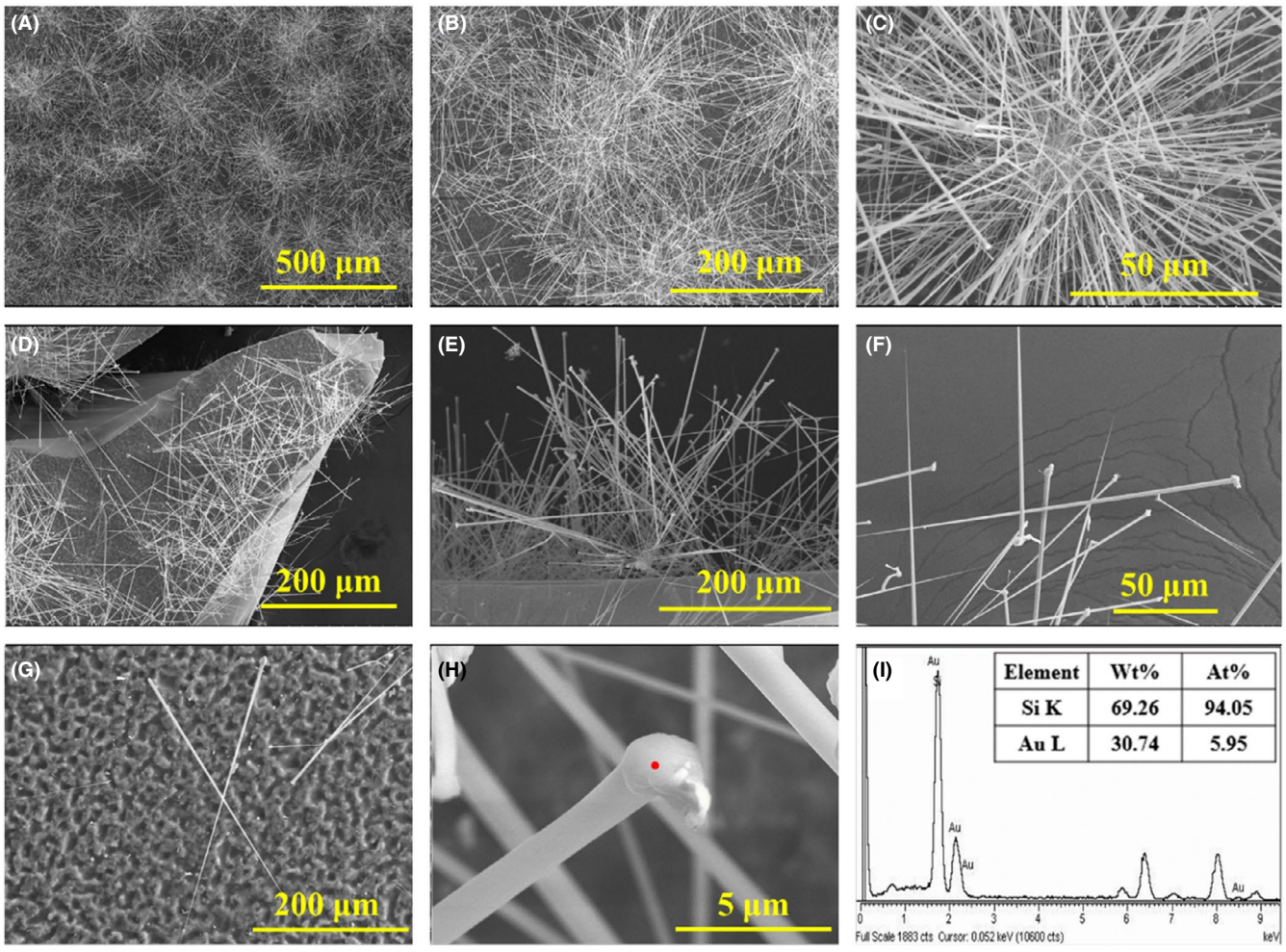

FIGURE 3 (A-H) Different magnification FESEM images of as-grown nanoneedles. (I) EDS spectrum of the top [Color figure can be viewed at wileyonlinelibrary.com]

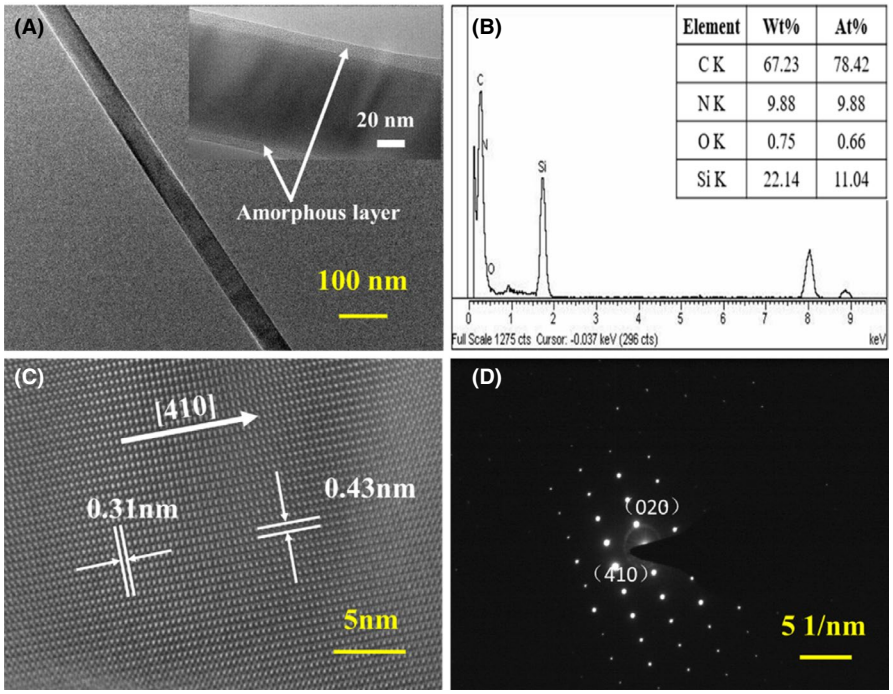

FIGURE 4 (A) TEM image of a single nanoneedle tip at low resolution. (B) EDS spectrum of α-Si_3N_4 nanoneedles. (C) A higher magnification TEM image of as-prepared α-Si_3N_4 nanoneedles. (D) Corresponding fast Fourier transform pattern [Color figure can be viewed at wileyonlinelibrary.com]

dispersed onto a TEM grid. Figure 4A shows a TEM image of a single nanoneedle tip. The diameter of the nanoneedle tip is about 42 nm. The inset in Figure 4A is an HRTEM image, revealing that the as-prepared α-Si_3N_4 nanoneedles possess a core-shell nanostructure. The chemical composition of a single nanoneedle tip was analyzed by EDS as shown in Figure 4B. The EDS spectrum shows Si, N, O, and C. Carbon is derived from the TEM carbon-supported carrier film. The as-detected Si, N, and O confirmed the α-Si_3N_4@SiO*x* core-shell structure. The oxygen comes from the residual air in the reaction system. Figure 4C,D shows a typical HRTEM image and the corresponding SAED pattern recorded from the α-Si_3N_4 needle region. These results further confirmed the single-crystalline feature of the nanoneedles. As can be seen, the lattice spacing observed is 0.31 and 0.43 nm, which corresponds to the (410) and (020) planes of α-Si_3N_4, respectively. The SAED pattern shown in Figure 4D can also be indexed to the α-Si_3N_4.

The PL spectrum was measured at room temperature in order to investigate the optical properties of the as-prepared α-Si_3N_4 nanoneedles. Excited by 254 nm UV light, the as-recorded emission spectrum from the nanoneedles is shown in Figure 5. An emission peak centered at 400 nm can be observed, which is located in the violet-blue spectral range. To further analyze the optical properties of the as-synthesized α-Si_3N_4 nanoneedles, the PL spectrum was simulated by the Gaussian-Lorentzian method. The black line is the intrinsic emission spectrum of α-Si3N4. The red one is the simulated line. The three short dash lines are the decomposition of the experimental peak into Gaussian components. The black emission spectrum shows three emission peaks

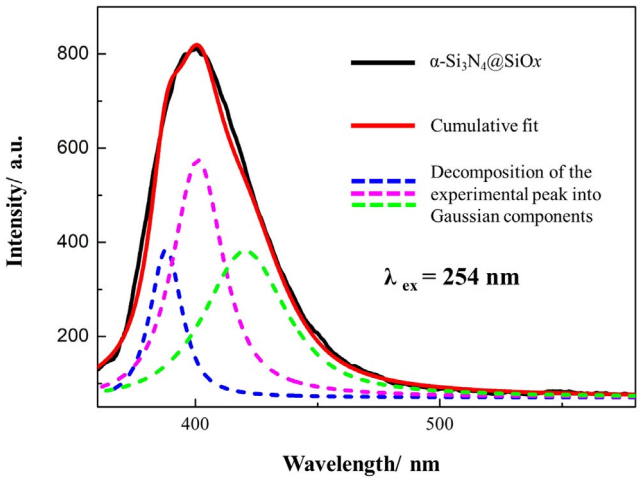

FIGURE 5 Emission spectra of α-Si_3N_4 nanoneedles and decomposition of the experimental peak into Gaussian components [Color figure can be viewed at wileyonlinelibrary.com]

at 388, 400, and 420 nm located in the violet/blue spectral range. Compared with α-Si_3N_4 nanowires (emission spectrum-417 nm) by Liu et al.,[32] there is a certain blue shift in the strong emission peak 400 nm and has two another weak emission peak at 388 and 420 nm. This is due to the difference in needle-like morphology, which makes more defects in the structure. Photoexcitation and luminous emission occur between all permissible energy states in the defective α-Si_3N_4 layer.[38] The prepared sample possesses a large amount of ≡Si - Si≡, and the presence of trace oxygen breaks the ≡Si - Si≡ chain in the α-Si_3N_4 nanoneedle energy gap, forming more Si - O - Si structural defects that cause electron radiative transitions.

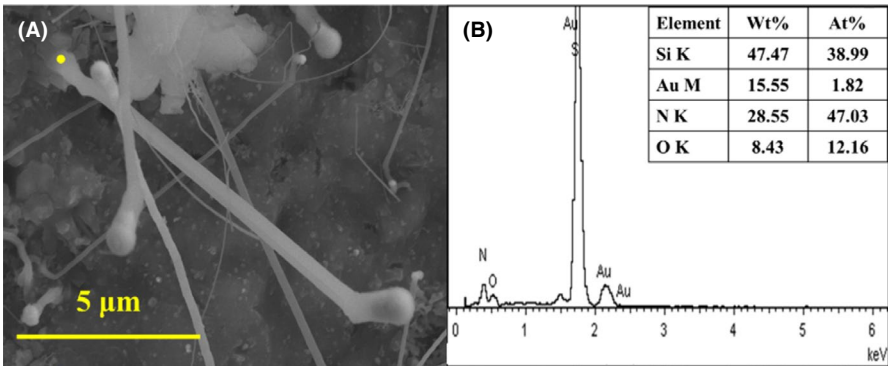

FIGURE 6 (A) FESEM image of α-Si_3N_4 prepared at 1100°C (B) EDS of (A) [Color figure can be viewed at wileyonlinelibrary.com]

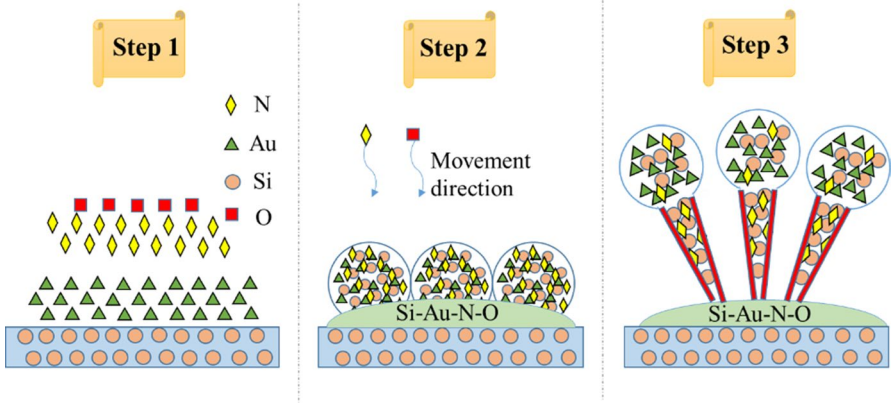

FIGURE 7 The growth mechanism of α-Si_3N_4 nanoneedles [Color figure can be viewed at wileyonlinelibrary.com]

The growth of one-dimensional nanostructure materials is traditionally governed by the mechanism of VLS (Vapor-Liquid-Solid), VS (Vapor-Solid), and SLS (Solid-Liquid-Solid) processes. In order to clarify the growth mechanism of the nanoneedles, an SEM image of the silicon nitride sample prepared at 1100°C is shown in Figure 6A.

When the temperature is raised to 1100°C, short α-Si_3N_4 nanowires can be obtained instead of nanoneedles, which can provide some useful clues for the initial formation process of the needle-shaped α-Si_3N_4. Their roots contain Si and Au, as revealed by EDS, shown in Figure 6B and Figure 3I, suggesting that VLS base-growth is in operation.

Figure 7 shows a schematic illustration for the growth of α-Si_3N_4 nanoneedles. As the temperature increases, Si and Au begin to melt at the contact surface to form a eutectic liquid phase, providing nucleation and active sites for the formation of nanoneedles. The employment of catalysts dramatically decreased the barrier of nucleation. Low supersaturation of the gas precursors enabled the growth of 1D nanomaterials along the low energy lattice plane. In this experiment, when maintaining at 1200°C, Si reacts with the limited amount of oxygen remaining in the air in the furnace chamber to form a small amount of solid SiO_2 by the reaction (1). At the same time, gaseous SiO is generated by a solid-solid reaction between Si and SiO_2 (reaction 2)[39,40]. The gas phase produced by the raw materials is continuously diffused into the Si/Au eutectic alloy clusters to form the Si-Au-N-O liquid droplets. When the Si-Au-N-O liquid droplets are supersaturated, nucleation will begin in the droplets. During the growth, part of Si-Au-N-O liquid droplets will gradually separate from Si substrate because of their poor wettability, becoming the caps of nanoneedles. Each single cap continuously absorbs SiO and N_2 to maintain stable growth, illustrated as the VLS cap-growth. At the same time, the other part of droplets on the substrate also contain Si and Au catalyst, becoming nanoneedle roots, implying that VLS base-growth contributes to the nanoneedle formation. Each root provides growth driving force for several nanoneedles, resulting in a less stable growth than caps. Due to the limited N_2 in the system, after the initial nanoneedle formation (reaction 3), when N_2 concentration is getting smaller, the growth driving force of the nanoneedles is insufficient and will become finer. Based on the above discussion, it is suggested that the overall growth mode of α-Si_3N_4 nanoneedles in this catalytic synthesis process is presumably governed by the combined VLS base-growth and VLS cap-growth mechanism.

$$Si_{(s)} + O_{2(g)} = SiO_{2(s)} \quad (1)$$

$$Si_{(s)} + SiO_{2(s)} = 2SiO_{(g)} \quad (2)$$

$$3Si_{(s)} + 2N_{2(g)} = Si_3N_{4(s)} \quad (3)$$

In this closed reaction system of the whole experiment, residual SiO gas reacts with oxygen to form viscous SiO_2, which is coated on the surface of the as-grown α-Si_3N_4 nanoneedles. As the melting point of α-Si_3N_4 is higher than that of SiO_2, the solidification of the α-Si_3N_4 core happens faster than that of the viscous SiO_2 layer. For this reason, a thin amorphous SiO_2 shell will be formed and wraps the crystalline α-Si_3N_4@SiO*x* nanoneedles.[41]

4 | CONCLUSION

Needle-like, single-crystal, α-Si_3N_4 nanoneedles have been prepared by using an improved, simplified, vapor-liquid-solid (VLS) method at 1200°C for 3 hours without using gases. The synthesized α-Si_3N_4 nanoneedles were 100-200 μm in length, evenly tapered from the cap to the root, whose diameter ranging from tens of nanometers to several micrometers through one nanoneedle. The resulting α-Si_3N_4 nanoneedles were structurally characterized and found to have α-Si_3N_4@SiO*x* core-shell nanostructures with a single-crystal α-Si_3N_4 core and an insulating amorphous silicon oxide shell. The formation of α-Si_3N_4@SiO*x* nanoneedles is supposed to be governed by the combined VLS base-growth and VLS cap-growth mechanism. Furthermore, α-Si_3N_4 nanoneedles prepared by this way have an emission peak at 400 nm under the excitation of 254 nm UV light. This result indicates that the morphology has a certain influence on the optical properties of the nanoneedles, and has potential applications in the optical fields such as UVC photodetectors.

We believe that this CVD method with Au layer evaporated on Si substrates to synthesis α-Si_3N_4 nanoneedles could enlighten us on the morphology of one-dimensional nanomaterials by changing the type of catalyst and the conditions of the gas to be introduced, so as to adapt to different application requirements. For example, generally speaking, it is better for cylindrical nanowires to require a larger aspect ratio, but in the field of solar applications, tapered nanoneedle morphology is a good light absorber for solar cell applications. Hence, to pay more attention to the one-dimensional nanomaterials morphology and to study other growth parameters like temperature is a necessary way to produce appropriate nanomaterials of good quality.

ACKNOWLEDGEMENTS

This present work was supported by National Key R&D Program of China (2018YFC1901503) and the National Natural Science Foundations of China (Grant No. 51472222, 51372232).

CONFLICT OF INTERESTS

The authors declare no competing financial interests.

AUTHOR'S CONTRIBUTION

Xiulin Shen, Haitao Liu, Xianmei Zhang, and Zhaohui Huang conceived and designed the experiments. Xiulin Shen carried out the experiments. Xiulin Shen, Haitao Liu, Yangai Liu, Minghao Fang, Xiaowen Wu, and Xin Min analyzed the data and discussed the results. Xiulin Shen wrote the paper.

ORCID

Zhaohui Huang https://orcid.org/0000-0001-9599-923X
Yangai Liu https://orcid.org/0000-0003-3285-3967
Minghao Fang https://orcid.org/0000-0003-4646-9915
Xiaowen Wu https://orcid.org/0000-0002-5611-0626

REFERENCES

1. Wei Q, Xue C, Sun Z, Zhuang H, Cao W, Wang S, et al. Fabrication of large-scale α-Si_3N_4 nanotubes on Si(111) by hot-wall chemical-vapor-deposition with the assistance of Ga_2O_3. Appl Surf Sci. 2004;229(1–4):9–12.
2. Buchanan Q. Nanotube mystery. Nat Phys. 2017;13:416.
3. Li L, Wang JW, Zhong H, Hao LY, Abadikhah H, Xu X, et al. Novel α-Si_3N_4 planar nanowire superhydrophobic membrane prepared through in-situ nitridation of silicon for membrane distillation. J Membrane Sci. 2017;543:98–105.
4. Wang F, Jin GQ, Guo XY. Sol–gel synthesis of Si_3N_4 nanowires and nanotubes. Mater Lett. 2006;60(3):330–3.
5. Xiong L, Dai J, Song Y, Wen G, Qin C. Investigation of photoelectrical properties of α-Si_3N_4 nanobelts with surface modifications using first-principles calculations. Phys Chem Chem Phys. 2016;18(23):15686–96.
6. Xiong L, Dai J, Zhong B, Wen G, Song Y. Orientation and passivation-dependent stability and electronic properties of alpha-Si_3N_4 nanobelts. Phys Chem Chem Phys. 2014;16(44):24266–74.
7. Huang J, Liu Y, Huang Z, Fang M, Zhang S, Xie W, et al. $Ni(NO_3)_2$-assisted catalytic synthesis and photoluminescence property of ultralong single crystal sialon nanobelts. Cryst. Growth Des. 2012;13(1):10–4.
8. Yue H, Wang X, Tian J. Fabrication of Si_3N_4 reticulated porous ceramics reinforced by needle-like β-Si_3N_4. Ceram Int. 2014;40(6):8525–32.
9. Cui H, Stoner BR. Nucleation and growth of silicon nitride nanoneedles using microwave plasma heating. J Mater Res. 2011;16(11):3111–5.
10. Meng Q, Li S, Kang Y, Zhai X, Wei S, He H, et al. Electrical and optical properties of nano aluminum film/particle structure. J Wuhan Univ Technol-Mater Sci Ed. 2017;32(5):989–93.
11. Guo Y, Li J, Chai S, Yao J. Nanomaterials for the optical detection of fluoride. Nanoscale. 2017;9(45):17667–80.
12. Oliveira DA, Silva JV, Flauzino JMR, Castro ACH, Moco ACR, Soares M, et al. Application of nanomaterials for the electrical and optical detection of the hepatitis B virus. Anal Biochem. 2018;549:157–63.
13. Wan W, Luo J, Yang J, Feng Y, Ouyang Y, Chen D, et al. High-temperature ablation properties of nano zirconia reinforced fused silica ceramics. Ceram Int. 2018;44(6):7273–5.

14. Nurbaiti U, Darminto Triwikantoro, Zainuri M, Pratapa S. Synthesis and characterization of silica sand-derived nano-forsterite ceramics. Ceram Int. 2018;44(5):5543–9.
15. Huang J, Miao Y, Zhang M, Feng Z, Hu Z, Li X, et al. Hot-pressed sintered Ca-α-Sialon ceramics with grains from short prismatic to elongated morphology synthesized via carbothermal reduction and nitridation. J Alloy Compd. 2018;767:90–7.
16. Xu K, Gao Z, Zhang R, Fu G, Xu C, Mao Y. Investigation of electron device based low dimensional nano structures. Integr Ferroelectr. 2018;188(1):79–87.
17. Kodali M, Herrera S, Kabir S, Serov A, Santoro C, Ieropoulos I, et al. Enhancement of microbial fuel cell performance by introducing a nano-composite cathode catalyst. Electrochim Acta. 2018;265:56–64.
18. Han B, Zhang L, Zeng S, Dong S, Yu X, Yang R, et al. Nano-core effect in nano-engineered cementitious composites. Compos A. 2017;95:100–9.
19. Nadiv R, Shachar G, Peretz-Damari S, Varenik M, Levy I, Buzaglo M, et al. Performance of nano-carbon loaded polymer composites: dimensionality matters. Carbon. 2018;126:410–8.
20. Paladiya C, Kiani A. Nano structured sensing surface: significance in sensor fabrication. Sens Actuators, B. 2018;268:494–511.
21. Nikfarjam A, Hosseini S, Salehifar N. Fabrication of a highly sensitive single aligned TiO_2 and gold nanoparticle embedded TiO_2 nano-fiber gas sensor. ACS Appl Mater Interfaces. 2017;9(18):15662–71.
22. Cheng W, Ju Y, Payamyar P, Primc D, Rao J, Willa C, et al. Large-area alignment of tungsten oxide nanowires over flat and patterned substrates for room-temperature gas sensing. Angew Chem. 2015;54(1):340–4.
23. Moaddeli A, Abdollahi-Alibeik M. A nano magnetically mesoporous catalyst for the synthesis of propargylamine derivatives. J Porous Mat. 2017;25(1):147–59.
24. Gupta NK, Peng B, Haller GL, Ember EE, Lercher JA. Nitrogen modified carbon nano-materials as stable catalysts for phosgene synthesis. ACS Catal. 2016;6(9):5843–55.
25. Han IS, Seo DW, Kim SY, Hong KS, Guahk KH, Lee KS. Properties of silicon nitride for aluminum melts prepared by nitrided pressureless sintering. J Eur Ceram Soc. 2008;28(5):1057–63.
26. Li B, Chen J, Yan M, Su J, Sun J, Li Y. Investigation on morphology evolution and phase interactions of Fe-containing Si_3N_4 in vacuum high-temperature environment. Isij Int. 2015;56(2):189–94.
27. Lu X, Wei Y, Wang H, Wen J, Zhou J, Fan J. Porosity and oxide layer dependence of thermal shock behavior of porous silicon nitride ceramics. J Mater Sci Technol. 2014;30(12):1217–22.
28. Liu X, Yi X, Guo R, Li Q, Nomura T. Formation mechanisms of Si_3N_4 microstructures during silicon powder nitridation. Ceram Int. 2017;43(18):16773–9.
29. Chen D, Zhang B, Zhuang H, Li W. Combustion synthesis of network silicon nitride porous ceramics. Ceram Int. 2003;29(4):363–4.
30. Yao D, Xia Y, Zuo KH, Jiang D, Günster J, Zeng Y-P, et al. Porous Si_3N_4 ceramics prepared via partial nitridation and SHS. J Eur Ceram Soc. 2013;33(2):371–4.
31. Huang J, Zhang S, Huang Z, Liu YG, Fang M. Growth of α-Si_3N_4 nanobelts via Ni-catalyzed thermal chemical vapour deposition and their violet-blue luminescent properties. Cryst Eng Comm. 2012;15(4):785–90.
32. Liu H, Huang Z, Huang J, Fang M, Liu YG, Wu X, et al. Novel, low-cost solid-liquid-solid process for the synthesis of alpha-Si_3N_4 nanowires at lower temperatures and their luminescence properties. Sci. Rep. 2015;5:17250.
33. Wang X, Liu J, Cheng B, Yu J, Wang Q. Metal catalysis-free, direction-controlled planar growth of single-crystalline α-Si_3N_4 nanowires on Si(100) substrate. Nanotechnol. 2006;17(15):3989–93.
34. Chen Y, Guo L, Shaw DT. High-density silicon and silicon nitride cones. J Cryst Growth. 2000;210:527–31.
35. Yang W, Xie Z, Li J, Miao H, Zhang L, An L. Ultra-long single-crystalline alpha-Si_3N_4 nanowires: derived from a polymeric precursor. J Am Ceram Soc. 2005;88(6):1647–50.
36. Zheng CS, Yan QZ, Xia M, Ge CC. In situ preparation of SiC/Si_3N_4-NW composite powders by combustion synthesis. Ceram Int. 2012;38(1):487–93.
37. Kusunose T, Yagi T, Firoz SH, Sekino T. Fabrication of epoxy/silicon nitride nanowire composites and evaluation of their thermal conductivity. J Mater Chem A. 2013;1(10):3440–5.
38. Shuleiko DV, Zabotnov SV, Zhigunov DM, Zelenina AA, et al. Photoluminescence of amorphous and crystalline silicon nanoclusters in silicon nitride and oxide superlattices. Semiconductors. 2017;51(2):196–202.
39. Chen J, Wang X. Preparation of silicon nitride nanowires and dielectric properties. Asian J Chem. 2013;25(14):7986–8.
40. Huang Z, Liu H, Chen K, Fang M, Huang J, Liu S, et al. Synthesis and formation mechanism of twinned SiC nanowires made by a catalyst-free thermal chemical vapour deposition method. RSC Adv. 2014;4(35):18360–4.
41. Chen K, Fang M, Huang Z, Huang J, Liu YG. Catalytic synthesis and growth mechanism of SiC@SiO_2 nanowires and their photoluminescence properties. Cryst Eng Comm. 2013;15(44):9032–8.

How to cite this article: Shen X, Liu H, Zhang X, et al. Facile synthesis of α-Si_3N_4 nanoneedles and their photoluminescence properties. *Int J Appl Ceram Technol*. 2019;16:2373–2379. https://doi.org/10.1111/ijac.13259